Structural and thermodynamic properties of Ag-Co nanoclusters

T. Van Hoof and M. Hou
Laboratoire de Physique des Solides Irradiés et des Nanostructures, Université Libre de Bruxelles, Campus de la Plaine CP 234, Bd du Triomphe, B-1050 Brussels, Belgium
(Received 17 May 2005; published 27 September 2005)

The Metropolis Monte Carlo and molecular statics methods with a semiempirical embedded atom potential are used to study the structural and thermodynamic equilibrium states of Ag-Co isolated nanoparticles. The state parameters considered are size (from 200 to 3000 atoms), temperature (from 0 to 1500 K), and composition (from elemental Co to elemental Ag). A lower and an upper limit to the Co concentration is found for the occurrence of a core-shell structure. The lower limit results from a balance between Co-Co binding energy and the stress of the Ag lattice. The upper limit is a consequence of the wetting of the Co core by Ag. When the core-shell structure takes place, the Ag shell induces an expansion of the Co core of no more than 2% while the Co core induces an average contraction of the Ag lattice which is twice as large and is mainly taken over by the interfacial Ag atomic layer. Co cores melt at a temperature lower than 1500 K, which is not sensitive to the thickness of the Ag shell. Inside the Co cores, coexistence is found possible between a liquid layer surrounding a solid center and the thickness of the liquid layer is an increasing function of temperature. With increasing temperature, depending on its thickness, the Ag shell may undergo a crystal to amorphous transition followed by an amorphous to liquid transition. The former is caused by the Co core but proceeds from the Ag free surface. The melting temperature of the Ag shell is fairly lower than of the Co core, suggesting the possibility of core-shell nanoparticles with a solid core and a liquid shell.

DOI: 10.1103/PhysRevB.72.115434 PACS number(s): 61.46.+w, 61.43.Bn, 64.75.+g

I. INTRODUCTION

Nanoparticles are objects of intermediate size between the atom and the bulk materials. Consequently, all their properties, whatever thermodynamic, mechanical, structural, electronic, magnetic or optical are size dependent with behaviors limited by the atomic and the macroscopic scales. Many of them are reviewed.[1–3] These properties often scale with the cluster radius.[4] Specially stable structures for well-defined cluster sizes are known, corresponding to so-called "magic numbers" of atoms,[5] associated either with closure of electronic shells,[6] or with close packed geometrical shapes like truncated octahedrons (TO) and icosahedrons.[5,7–10] Among the huge variety of nanoparticles now available, metallic ones display original electronic and magnetic properties related to their structure or to their morphology, that might have technological applications provided they can be transferred to the macroscopic scale. To this purpose, particles need to be embedded in a matrix, deposited on a surface or assembled in a controlled way. For instance, magnetic structures are constructed by depositing clusters on a metallic surface,[11–13] and their properties result from a combination of the particle properties and their interaction with the environment.[14–18] A recent review is presented in Ref. 19, emphasizing the relation between magnetic properties and the structure of clusters and cluster assemblies. One interesting class of magnetic clusters is the class of bimetallic systems. Some, like CoPt display segregation enhanced by the large surface to volume ratio at the nanoscale and others, as an extreme case of segregation, may display core-shell structures.[20] This is the case of Ag-Co clusters. In bulk materials, phase diagrams provide the possible equilibrium alloy compositions. Nanophase materials may be formed accordingly, as reviewed in Ref. 21 and 22. On the other hand, the synthesis of nanoparticles can be achieved far from thermodynamic equilibrium, at elevated temperature, and then quenched into a metastable state which cannot be reached when synthesizing bulk materials. This way, it is thus possible to obtain phases at room temperature which are not present in the equilibrium phase diagrams. This is the case of the laser vaporization technique[21,23] which allows synthesizing clusters formed by non miscible elements like silver and cobalt.

The properties of bimetallic clusters strongly depend on the atomic organization of the different chemical species. In Ag-Co clusters, segregation of Ag at the surface is expected because the excess surface energy of Ag is lower than the one of Co.[24] The study of the optical properties of Ag-Co clusters embedded in an aluminium matrix confirms the core-shell structure.[25] Electron diffraction experiment on Ag-Co clusters deposited on amorphous carbon shows that Ag and Co are crystallized in their own fcc structure, which also confirms phase separation.[26] However x-ray absorption measurements on Ag-Co clusters embedded in a MgO matrix indicate that the Ag shell might not be complete. XPS measurement on Ag-Co clusters deposited on amorphous Si tend to confirm this result.[27] Generally, bimetallic clusters synthesized by laser vaporization display broad cluster size and composition distributions.[26,27] Sizes range from a few atoms to a few thousand atoms and all compositions are possible. Both distributions may influence cluster properties, and thus the core-shell structure, since, as is shown below, the detail of the atomic arrangement depends on size and on composition. Atomic scale modelling is a powerful tool for predicting the atomic configurations of individual clusters. *Ab initio* calculations on the very small $Ag_{10}Co^{+}$ cluster predict the Co atom to sit in the cluster center.[28,29] This may be the smallest possible Ag-Co core-shell cluster. In the case of bigger ones,

TABLE I. Matrix of parameters.

Size	200	500	1000	1500	2000	2500	3000
X_{Co}	0.0	10Co	0.1	0.25	0.5	0.75	1.0
T(K)	100	300	600	900	1200	1500	

for the sake of computer efficiency, classical modelling methods using semiempirical potentials are used. In clusters formed by nonmiscible elements, core-shell[30] or or even onionlike structures[31] have been predicted with classical molecular dynamics simulations. The latter are probably the consequence of the absence of a likely kinetic path toward equilibrium. The Metropolis Monte Carlo method (MMC) allows sampling configurations for minimizing the free energy of a system, irrespective to its temporal evolution. This method was used to show the composition dependence of Co_nAg_{201-n} clusters with TO shapes. A core-shell structure is found for $50<n<79$ and not for other compositions.[32] The question addressed in this work, more generally, is to determine the dependence of the equilibrium cluster structure on size, composition, and temperature. This step is necessary for understanding the modification of the cluster state when embedded in a matrix or deposited on a surface, taking the interaction with its environment into account. The systems studied and the MMC model are presented in Sec. II. The results are presented and discussed in Sec. III and a conclusion is given in Sec. IV.

II. MODELLING

A. Modelling tools

The atomic structure of clusters is studied as a function of size, composition and temperature, in a realistic range. Sizes from 200 to 3000 atoms are considered, that are currently obtained by laser vaporization techniques. The compositions are chosen in the whole range from elemental Co to elemental Ag and the temperatures range from 100 K to 1500 K, covering the solid state and melting. The number of atoms in the clusters considered is small enough to allow modelling them at the atomic scale. In this work, we focus on their equilibrium state rather than on their evolution toward equilibrium. Therefore, time is no relevant parameter and MMC is a suitable technique. A limited number of different sizes, compositions and temperatures are considered that are given in Table I. Despite the limitation, this represents a huge series of simulations (294 cases) to which further calculations are added by spot when finer tuning is necessary for discussion. The MMC importance sampling method is well documented[33,34] and is used to predict the equilibrium atomic configuration of bimetallic Ag-Co free clusters. The equilibrium configuration of a system is defined as the configuration with the lowest free energy. The MMC sampling is achieved in the canonical ensemble (NVT). The sampling scheme includes two types of trials. (i) Random displacement of each atom in the cluster from each current position. (ii) Random site exchange between two chemically different atoms. A trial is accepted if it lowers the configuration energy of the system. If the configuration energy is increased, trials are accepted as well with a probability proportional to a Boltzmann factor,

$$P = e^{-\Delta U/kT}, \tag{1}$$

where ΔU is the configuration energy difference. The magnitude of the moves in (i) is dynamically adjusted in order to maintain a rate of acceptance close to 0.4, which is empirically found to optimize convergence. Trials (ii) correspond to no physical path of the system but are used for limiting the risk of trapping the system into a local minimum as well as for enhancing convergence. In the present work, 5×10^6 MMC steps are used in each simulation. It is generally sufficient for the system to converge to equilibrium, which was checked by repeating several simulations using different initial conditions. In principle, the equilibrium state of the system is independent of the initial conditions. Their choice however makes the MMC algorithm more or less efficient. Convergence of the MMC algorithm is optimized by a preliminary relaxation of the initial atomic positions at 0 K. In the the molecular statics (MS) algorithm, the trajectories of each atom in the system are calculated with the classical Newton equation of motion using the Verlet algorithm.[33,34] The force acting on each atom is derived from the same interatomic potential as used in MMC. At each step, if the scalar product between the instantaneous velocity and the force acting on an atom is negative, the velocity is set to zero. This way, a relaxed configuration of the cluster at 0 K, close to the initial state, with a few integration steps. In what follows, MS simulations are also used to estimate excess energies at 0 K. Except when mentioned, the initial cluster morphology is assumed spherical and the atomic positions form a perfect fcc lattice with the lattice parameter of bulk silver (4.09 Å). This is a nonequilibrium configuration and the equilibrium state is determined by MS followed by MMC at the desired temperature.

A semiempirical embedded atom model potential is used, which has the advantage of a simple mathematical expression allowing fast computations of configuration energies.[35] The expression of the cohesive energy is given by

$$E_i = \frac{1}{2}\sum_{j\neq i} V_{\alpha\beta}(r_{ij}) - F_\alpha(\rho_i), \tag{2}$$

where the electronic density ρ_i at site i is given by

$$\rho_i = \sum_j \psi_j(r_{ij}). \tag{3}$$

Binding energy is described by F_α, a functional of the local electronic density of the host, ρ_i. This functional is parameterized on the equation of states of Rose[36] and only the repulsive component of the configuration energy, which warrants the crystal structure stability, needs further fitting.[37] In this potential, only the repulsive part contains a mixed term $V_{\alpha\beta}$. The mixed repulsive interaction is expressed as a weighted average of the pure repulsive components $(V_{\alpha\alpha}, V_{\beta\beta})$.[37] This approximation has no strong physical grounds. It was however successfully applied to calculate heat of solutions in binary alloys made of Au, Cu, Ag, Ni,

Pd, and Pt.[37,38] In the present work, one additional parameter is allowed for tuning the strength of this weighted average. In the case of Ag-Co systems however, the weighted average suggested in Ref. 37 was found satisfactory. The potential was assessed by comparing the calculated and measured values of substitutional Co to first Ag neighbor distance in Ag, of the Ag-Co distance at the interface between a Co cluster and a Ag matrix at low temperature, as well as of Debye temperatures associated with the vibrations of a substitutional Co and of Co clusters embedded in the same Ag matrix.[39]

B. The analysis tools

The cluster properties we are interested in are segregation, short and long range order and diffusion. These are described by quantities whose expectation values can be computed as equilibrium thermodynamic averages by MMC sampling. The segregation is studied by means of a radial density distribution, $\rho(r)$, using the cluster center as a reference origin. It is calculated separately for the Ag and the Co subsystems. Structural properties are measured by means of a pair correlation function $g(r)$ given by

$$g(r) = \frac{1}{N(N-1)} \sum_{i=1}^{N-1} \sum_{j>i}^{N} \delta(r - r_{ij}), \tag{4}$$

where N is the number of atoms in the cluster and r_{ij} the dustance between atoms i and j. The average first neighbor distance d is the modal position of the first peak, estimated after background substraction when necessary. The distance d is used to measure the relaxation of the atomic positions in the bimetallic clusters as relative to its value in bulk materials or elemental clusters. The properties of the second, third and fourth peaks in $g(r)$ are used to characterize the crystalline state as well as phase transitions. To this purpose, and also for discussing phase separation in Ag-Co clusters, $g(r)$ is calculated separately for the Ag and the Co subsystems. During simulations, the $\rho(r)$ and $g(r)$ histograms are constructed with an bin size of 8×10^{-3} Å. When better resolution is necessary, the peak positions are obtained by fitting their central part to a Gaussian function. Mean square atomic displacements of atoms are used to evidence diffusion. They are measured at a given MMC step as an ensemble average of the atomic positions,

$$\langle \delta r^2 \rangle = \frac{1}{N} \sum_{i=1}^{N} (\langle r_i^2 \rangle - \langle r_i \rangle^2), \tag{5}$$

where r_i is the current position of atom i. In the solid state $\langle \delta r^2 \rangle$ is a constant representing the mean square atomic thermal vibration amplitude. When diffusion occurs, $\langle \delta r^2 \rangle$ increases continuously with the step number and is only limited by the finite size of the cluster. Because of the small size of clusters, their surface play an important role in the their properties. The fraction of surface atoms is measured as the ratio, noted S/V, of atoms with coordination $Z<12$ and atoms with coordination $Z=12$ (in the perfect fcc structure, atoms have 12 first neighbors, except at surfaces where their number is lower). In the case of phase separation, both surfaces and interfaces are characterized by excess energies and related quantities. The 0 K excess energy of a cluster ΔE_C is defined as follows:

$$\Delta E_C = E_C - E_C^{\mathrm{Id}} \tag{6}$$

where E_C is the configuration energy of the cluster with a given size and stoichiometry at 0 K. E_C^{Id} is the energy per atom of an infinite ideal solid solution with the same stoichiometry,

$$E_C^{\mathrm{Id}} = \frac{1}{N_{\mathrm{Co}} + N_{\mathrm{Ag}}} [N_{\mathrm{Co}} E_C(\mathrm{Co}) + N_{\mathrm{Ag}} E_C(\mathrm{Ag})], \tag{7}$$

where $E_C(\mathrm{Co})$ and $E_C(\mathrm{Ag})$ are, respectively, the bulk cohesive energies of Co and Ag extrapolated at 0 K. N_{Co} and N_{Ag} are, respectively, the number of Co and Ag atoms. One useful related quantity is the excess energy as relative to an ideal solution cluster. The excess energy of an ideal mixed cluster $\Delta E_C^{\mathrm{IdCl}}$ is here defined as a linear combination of the the excess energies of elemental clusters,

$$\Delta E_C^{\mathrm{IdCl}} = \frac{1}{N_{\mathrm{Co}} + N_{\mathrm{Ag}}} [N_{\mathrm{Co}} \Delta E_C^{\mathrm{Cl}}(\mathrm{Co}) + N_{\mathrm{Ag}} \Delta E_C^{\mathrm{Cl}}(\mathrm{Ag})], \tag{8}$$

where $\Delta E_C^{\mathrm{Cl}}(X)$ is the excess energy of an elemental cluster containing N_X atoms.

III. RESULTS AND DISCUSSIONS

This section is organized in two subsections. In the first, the factors governing the segregation and phase separation between Ag and Co are identified and discussed in terms of excess energy. A condition for the transition between spherical and faceted cluster morphologies is identified. The second subsection focuses on the cluster structure in conditions where phase separation takes place. The cases of the Co and Ag subsystems are considered separately.

A. Segregation

1. Influence of size and composition

The spatial distribution of Co and Ag in clusters depends on their size and composition. This is illustrated by Fig. 1, where $\rho(r)$ is displayed for two 500 atoms equilibrium clusters: $Ag_{490}Co_{10}$ and $Ag_{375}Co_{125}$, at 300 K. In the case of the $Ag_{375}Co_{125}$ cluster, the cobalt is regrouped at small r while silver is located at larger r values. A clear partition takes place where Co forms a core surrounded by a Ag shell. A different situation is observed in the $Co_{10}Ag_{490}$ cluster. Here, cobalt is located between the cluster center and its surface formed by Ag exclusively. In this case, the radial density distribution provides no information about the possible grouping of Co atoms in precipitates and snapshots of the equilibrium cluster configurations are examined therefore. Figure 2 shows that Co atoms form one single group just beneath the surface and confirms the core-shell structure of the $Ag_{375}Co_{125}$ cluster. In order to explain this difference, the 300 K configurations of the clusters are quenched to 0 K. For the $Ag_{490}Co_{10}$ cluster, the 0 K configuration energy is

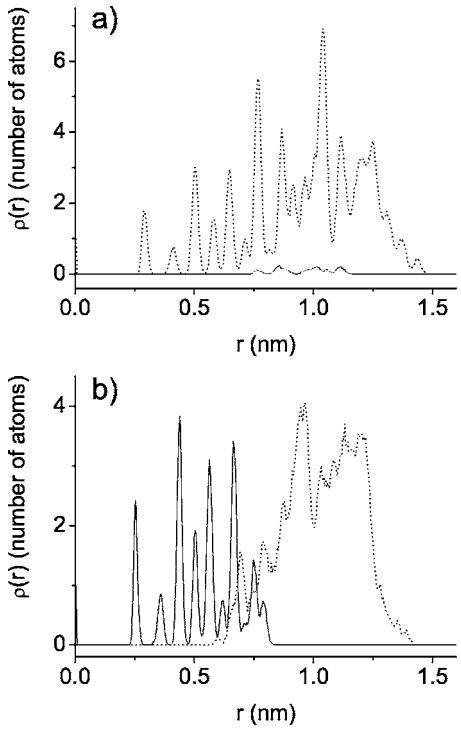

FIG. 1. $\rho(r)$ in the $Co_{10}Ag_{490}$ (a) and $Co_{125}Ag_{375}$ (b) at 300 K. Contributions of Co and Ag are represented, respectively, by straight and dotted lines.

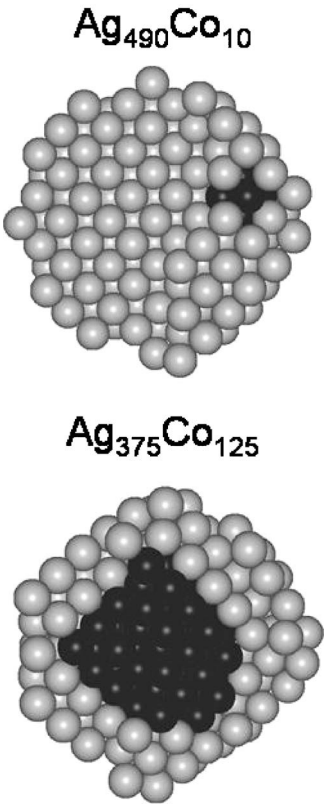

FIG. 2. Snapshot of the final configuration of the $Co_{10}Ag_{490}$ and $Co_{125}Ag_{375}$ clusters. Planar cuts through the clusters centers are shown. Co and Ag atoms are represented by dark and light spheres, respectively.

compared with the configuration energy of a cluster of the same composition, but with a core-shell structure. The former, $E_{\mathrm{Eq}}=-2.5935$ eV/atom, is lower than the latter, $E_{\text{Core-Shell}}=-2.5905$ eV/atom. We now distinguish between the Ag and the Co subsystems and find that the same relation applies for the 0 K configuration energy of the Ag subsystem [$E_{\mathrm{Eq}}(\mathrm{Ag})=-2.5732$ eV/atom $<E_{\text{Core-Shell}}(\mathrm{Ag})=-2.5680$ eV/atom]. However, the opposite relation is found in the Co subsystem [$E_{\text{Core-Shell}}(\mathrm{Co})=-3.6952$ eV/atom $<E_{\mathrm{Eq}}(\mathrm{Co})=-3.5856$ eV/atom]. The relation for the Co subsystem is explained by the lowering of the average coordination when it is located close to the surface. The situation in the Ag subsystem is more complex. Since a large mismatch exists between Ag and Co equilibrium lattice distances, strong relaxation takes place at the Ag-Co interface, involving large excess energy, mainly stored in the relaxation of the Ag subsystem. In the case of multilayers, the consequences of this mismatch are well-known configurations.[40] In the present simulations, relaxation is determined by measuring the mean Ag-Ag first neighbor distance. It is found closer to the bulk value (2.89 Å) in the equilibrium configuration (2.87 Å) than in the core-shell structure (2.86 Å). This indicates that the Ag lattice relaxation due to the presence of Co is larger in the core-shell structure and, as a consequence, the configuration energy of the Ag subsystem is higher. Since there are only few Co atoms in the system, at equilibrium, the higher energy stored in the Co subsystem is balanced by the lower energy stored in the Ag subsystem as compared to the core-shell case. This balance reverses when the number of Co atoms is increased since the additional Co-Co binding decreases the energy per atom stored in the Co subsystem and the core-shell structure becomes more favorable. Similar composition dependence of the spatial distribution is obtained for each cluster size at room temperature. The lowest Co concentration necessary to obtain a core-shell structure is 25% for clusters containing 200 and 500 atoms. In clusters containing more than 1000 atoms, the energy balance favors the core-shell structure when the Co concentration is 10% or more. Since only 5 different compositions are considered for each cluster size, the present results do not allow predicting the intermediate composition structures as a function of size accurately. It is found however that for clusters of all sizes containing no more than 10 Co atoms, these ones always regroup beneath the cluster surface. In order to extrapolate this observation to larger systems, MMC simulations are performed, predicting the position of 10 Co atoms in an infinite crystalline Ag layer with 8 lattice parameter thickness containing two free (100) surfaces. The simulation box is cubic and periodic boundary conditions are applied parallel to the (100) surfaces. Here again, at equilibrium, the 10 Co atoms precipitate into one single group just beneath the surfaces. The atomic organization within the clusters is found independent of temperature, up to melting. The previous results show the occurrence of a low Co concentration limit for obtaining an equilibrium core-shell structure. An upper limit is observed too, related to simple geometrical considerations about the fraction of surface atoms, S/V. Consistently with a Frank-van der Merwe growth mode, it is found that silver

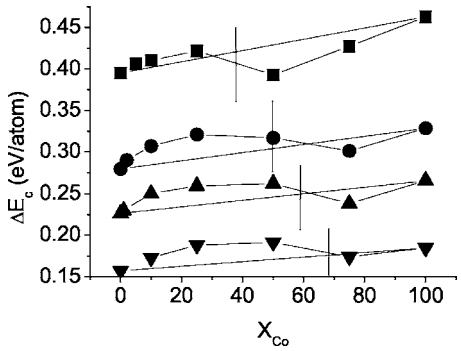

FIG. 3. Excess energies of equilibrium clusters as functions of the Co atomic fraction. Squares, circles, triangles on the edge and on the tip represent the results for concerning the 200, 500, 1000, and 3000 atoms clusters, respectively. The vertical lines indicate S/V for each cluster size, as calculated for spherical clusters.

forms no island on the Co cluster surface and builds up one single monolayer as soon as its fraction gets equal to S/V.

2. The origin of Ag segregation

In order to study the conditions for the formation of a Ag monolayer in deeper detail, we calculate the excess energy of the equilibrium clusters with respect to an ideal Ag-Co solution, ΔE_c (6). Figure 3 shows ΔE_c as a function of the Co concentration for different cluster sizes. Two different features come out, both contributing to the formation of the Ag surrounding layer. The first feature comes out the examination of the excess energy of elemental clusters. It is positive, as a consequence of the occurrence of the curved free surface and it scales with the inverse of the cluster radius (not shown in Fig. 3). The excess energy of the elemental Ag clusters is lower than the one of elemental Co clusters of the same size, indicating that the segregation of Ag to the surface of mixed Co-Ag clusters is energetically favorable. The second feature in Fig. 3 comes out of the examination of the excess energies in the mixed clusters, compared to hypothetical ideal solution clusters.

Deviations from the scaling law occur in this case that are not expected in ideal solution clusters. In Fig. 3, $\Delta E_c^{\mathrm{IdCl}}$ (8) is represented for each cluster size by a solid straight line connecting the energy of the pure Co and Ag clusters. We observe $\Delta E_c > \Delta E_c^{\mathrm{IdCl}}$ for small Co concentration and the opposite relation for high Co concentration. The Ag concentration where $\Delta E_c = \Delta E_c^{\mathrm{IdCl}}$ is close to S/V whatever the cluster size (vertical lines in Fig. 3). S/V, obtained on the basis of a coordination analysis of the atoms in the clusters is given in Table II for the different cluster sizes investigated. A small offset is observed which comes from the larger atomic radius of Ag as compared to Co, inducing an increase of the Co concentration required for obtaining a Ag monolayer with respect to the value of S/V in elemental clusters. For low Co concentration, $E_c < E_c^{\mathrm{IdCl}}$ is merely the energetic evidence of the nonmiscibility of Ag and Co. The opposite energetic relation observed for high Co concentration is the indication of the wetting of the Co core by the Ag atoms.

TABLE II. Fraction of surface atoms in elemental spherical clusters of different sizes.

Size	200	500	1000	3000
S/V	62.5	50	41	32

3. Relation between composition and morphology

The initial cluster configurations are spherical. After MMC minimization, the spherical shape is preserved. However, experiment shows that deposited and embedded nanoclusters may display facetted symmetrical shapes.[5,7,8] Clusters with a fcc lattice structure may form perfect truncated octahedra (TO) with {111} and {100} facets. The number of atoms in these clusters is thus well-defined and is given by the relation $N(n)=16n^3-33n^2+24n-6$ where n is a positive nonzero integer.[41] In a previous work, the atomic configuration of free Ag-Co clusters containing 201 atoms ($n=1$) with a TO morphology at room temperature was considered.[32] The TO morphology is interesting because it contains a lot of well-defined different possible atomic positions with different coordination numbers. These different sites may act as nucleation centers[9,10] and play a specific role in the atomic configuration of the mixed Ag-Co clusters. For instance, similarly to the spherical cluster morphology described above, in TO clusters with low Co concentration ($<20\%$), Co atoms were found to form small groups below the low coordination sites ($Z<9$), minimizing this way the configuration energy by minimizing the Ag lattice relaxation. At Co concentration higher than 50%, the Co regroups at the clusters center. Similarly, this composition effect comes from the balance between the energy of the Ag relaxation, and the cohesive energy of Co. The main difference with spherical clusters deals with the number of Co groups below the surfaces. While only one Co groups is observed below the surface of a 200 atoms spherical cluster containing 10 Co, in the TO clusters, the Co generally forms two different small groups located below two opposite lowest coordination {100} Ag facets. The cluster morphology may thus have an influence on the atomic arrangement in clusters, Co atoms being grouped close to well-defined low coordination Ag atom sites. An energy criterion can be found for predicting the spherical or facetted nature of the cluster morphology. This one comes out of Fig. 4. In this figure, the excess energies of the spherical and TO clusters containing 200 and 201 atoms, respectively, are compared at different compositions. For elemental clusters, ΔE_c is lower in the case of the TO than of the spherical shape. The fact that the number of atoms in both clusters differs by one unit has no effect on this result. This is due to the presence of well-defined higher coordination {111} facets than at the surface of a sphere. If, starting from an elemental Ag cluster, the amount of Co is increased, the excess energy of TO clusters increases up to a value close to that of the spherical clusters. Below 15% Co, when Co forms several small groups below the surface, the TO shape is the best stable. Between 15% and 40% Co, the excess energy of both shapes are close and the favored one cannot be predicted. For clusters containing between 50% and 80% Co, the spherical shape induces a lower excess energy than TO. For these compositions, ΔE_c of spherical clusters is

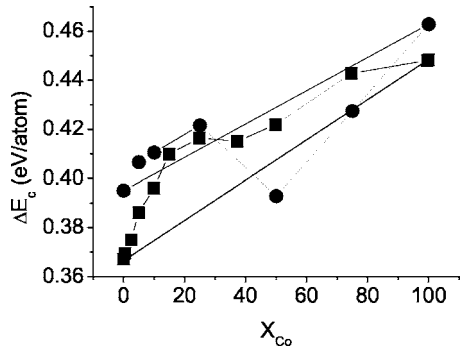

FIG. 4. Excess energies of TO and spherical clusters containing 201 and 200 atoms as functions of the fraction of Co atoms. Results for TO and spherical clusters are represented by squares and circles, respectively.

lower than of ideal solution spherical clusters. In the case of TO clusters, no such behavior is observed. The excess energy of TO clusters is always larger than of the ideal solution TO cluster. A small decrease of the excess energy is observed around 60% Co which corresponds to the formation of a single Ag monolayer around Co.

B. Structure

1. Lattice properties of the cobalt subsystem

a. Relaxations: As it comes out of the previous section, in most mixed clusters, Co forms a compact core surrounded by a Ag shell. The question is now addressed of the influence of the Ag shell on its structure. To this purpose, the relaxation of atomic Co positions in the cluster cores is compared to that in elemental spherical fcc Co clusters. Results are presented in Fig. 5, where $d_{\text{Co-Co}}$, the average Co-Co first neighbor distance, is reported for all the clusters studied as a function of the number of Co atoms in the core. The first neighbor distance in bulk fcc Co and in elemental fcc Co clusters are given for comparison. $d_{\text{Co-Co}}$ is always lower in pure clusters than in bulk fcc Co. As can be expected, since

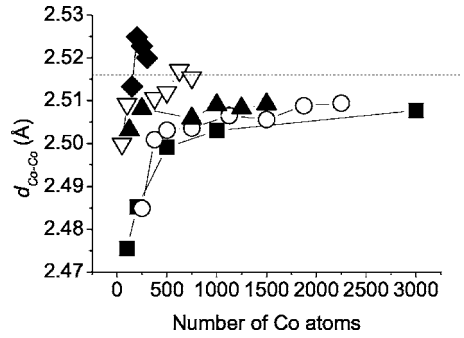

FIG. 5. $d_{\text{Co-Co}}$ in several clusters as a function of the number of Co atoms. Results are regrouped by clusters having Ag shells of equal thicknesses. Square on the edge represent $d_{\text{Co-Co}}$ in pure Co clusters. Circles, triangles on the edge, triangles on the tips and squares on the tip represent, respectively, the results in clusters with one, two, three, and four Ag atomic layers. The dotted line gives $d_{\text{Co-Co}}$ as predicted in bulk fcc cobalt.

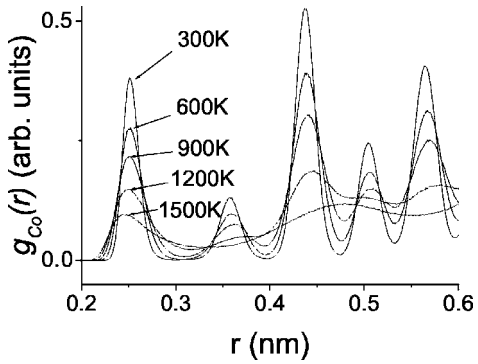

FIG. 6. $g(r)$ for Co atoms in a $Ag_{2250}Co_{750}$ cluster at different temperatures from 300 K to 1500 K.

S/V decreases with increasing cluster size, the difference between the bulk and the cluster values decreases as well and is to be assigned to the cluster surface contraction. The results in Fig. 5 are subdivided into groups of clusters having Ag shells of the same thickness. This way, the increase of $d_{\text{Co-Co}}$ with increasing Ag shell thickness is evidenced. One silver monolayer is not found inducing a large overall expansion of the Co lattice. Accumulating silver layers induces an increasing Co relaxation and, as seen in the case of the smallest Co cores, $d_{\text{Co-Co}}$ may even get larger than in bulk fcc Co. Thick Ag shells thus induce large strain in the Co cores and the magnitude of this strain correlates with the fraction of interfacial Co atoms. The Co relaxation exceeds 0.1% of $d_{\text{Co-Co}}$ in elemental Co clusters only for Co cores containing less than 500 Co atoms and surrounded by more than 2 Ag atomic layers. The largest Co lattice expansion observed is 2% of $d_{\text{Co-Co}}$ in elemental cluster.

*b. Melting:*This section focuses on the transition toward melting as the Co core temperature is increased. The case of Ag is different and will be addressed separately. Cluster melting is studied experimentally,[42–44] by classical Molecular Dynamics[45–49] and, as the smallest ones are concerned, *ab initio*.[50,51] Little is done for the case of mixed clusters and, in particular for core-shell clusters. One significant interest of the Ag-Co system is the large difference between bulk melting temperatures of the elemental species. In view of characterizing the melting of the Co cores, pair correlation functions and mean square atomic displacements are employed. Figure 6 displays the pair correlation function, $g(r)$, evaluated for Co atoms at several temperatures in a 3000 atoms cluster. The cluster contains 25% Co. Size and composition effects are considered next. Thermal displacements increase with temperature, making $g(r)$ peaks broader with increasing temperature and their amplitude lower. The part of the pair correlation function displayed is typical of the four first neighbor peaks in the fcc structure, which remains clearly visible up to temperatures of 1200 K. At 1500 K, the second and more distant neighbor peaks vanish. This is the signature of the disordering of the fcc structure and may indicate the melting of the Co core. Several features are consistent with melting, that are now discussed. Although the resolution is small [$g(r)$ is calculated at temperature intervals of 300 K only], the second peak is seen to vanish progressively with increasing temperature indicating that the solid-liquid phase

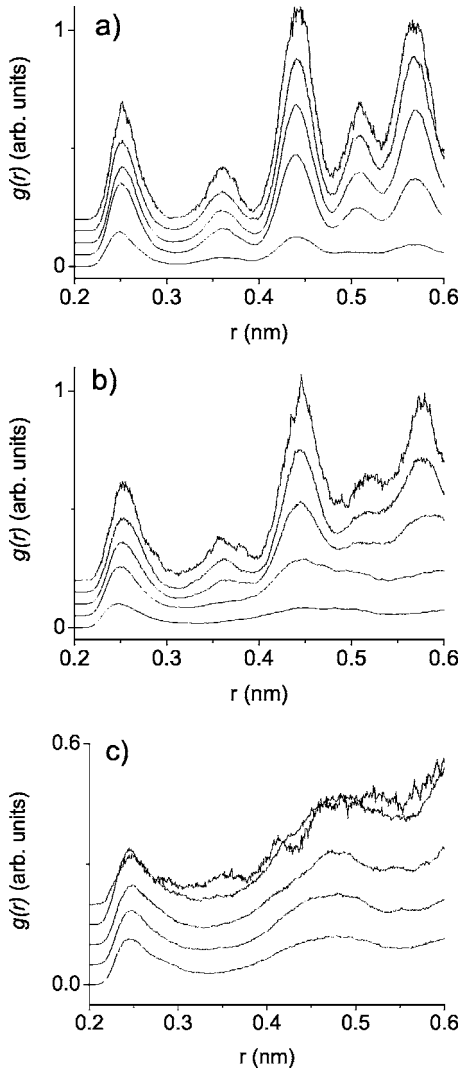

FIG. 7. $g(r)$ for Co atoms in different spherical layers with a thickness equal to 2.5 Å inside the same $Ag_{2250}Co_{750}$ cluster as in Fig. 8. In each graph, the upper curve corresponds to the central atoms layer and the lowest to the upmost layer. Results are shown at (a) 900 K; (b) 1200 K; and (c) 1500 K.

transition might be smooth. The reason is different, however. The detail of the melting appears better clearly in Fig. 7 $g(r)$ where is represented at different temperatures, as calculated in concentric spherical layers, starting from the cluster center up to the Ag-Co interface. The layer thickness is 2.5 Å (close to $d_{\text{Co-Co}}$). At 900 K, all the Co layers are ordered. At 1200 K, only the three deepest Co layers are ordered. The pair correlation functions in the other Co surrounding layers feature no second, third, and fourth neighbor peaks, indicating that they are liquid. At 1500 K, all layers are disordered. This is cross-checked by visualizing a slab in the last snapshot of the cluster, displayed in Fig. 8. Up to 900 K, the Co core has a visible crystalline structure. At 1200 K only the center of the Co core is crystalline. Some Co atoms are dissolved in the Ag surrounding layer. At 1500 K, the whole Co core is disordered. These results show that, in core-shell nanoclusters, the disordering of the core starts at the interface and proceeds toward the center as the temperature is increased. At intermediate temperatures, both phases coexist. A close examination of Figs. 6 and 7 indicates an additional signature of melting. According to the Lindeman criterion, melting starts when the fraction of diffusing atoms is high. Diffusion induces an overlap between the first and second neighbor peaks in the pair correlation function. In Fig. 6, it is strictly zero for temperatures of 300 K to 900 K. At 1200 K, the background between the two first peaks is as high as the amplitude of the second peak itself, as the result of an intense diffusion. Diffusion is also characterized by the mean square thermal displacement of the atoms, $\langle \delta r^2 \rangle$. $\langle \delta r^2 \rangle_{\text{Co}}$ is calculated for the Co subsystem in the same $Ag_{2250}Co_{750}$ cluster at different temperatures. The results are given in Fig. 9. Below 1200 K the $\langle \delta r^2 \rangle_{\text{Co}}$ is low and stable. The increase of equilibrium $\langle \delta r^2 \rangle_{\text{Co}}$ with increasing temperature corresponds to the increase of the mean square thermal vibration

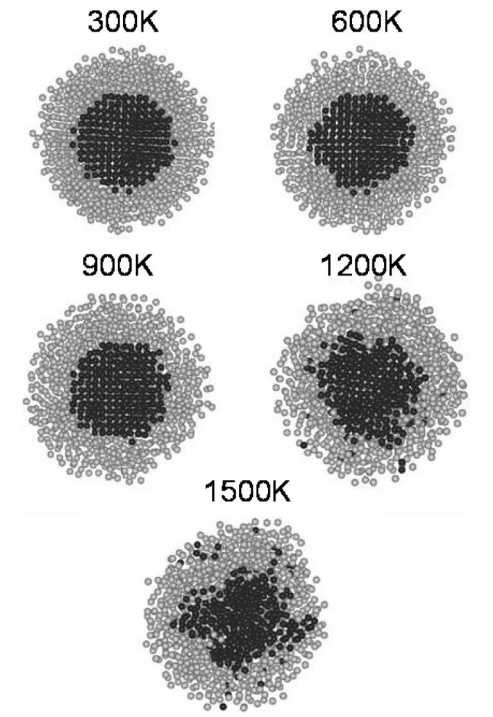

FIG. 8. Cuts through equilibrium $Ag_{2250}Co_{750}$ cluster configurations at several temperatures. Dark spheres: Co atoms; light spheres: Ag atoms.

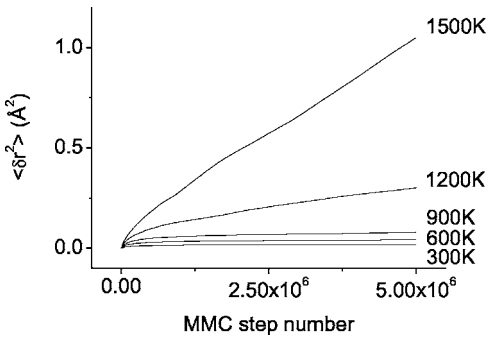

FIG. 9. Mean square displacement, $\langle \delta r^2 \rangle_{\text{Co}}$, in a $Ag_{2250}Co_{750}$ cluster as a function of the MMC step number at temperatures from 300 K to 1500 K.

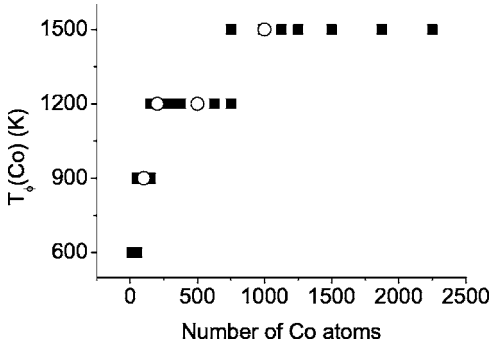

FIG. 10. T_ϕ(Co) as a function of the number of cobalt atoms. The results of all the simulations for all clusters size and composition are represented by squares. The open circles represent T_ϕ(Co) of elemental Co clusters.

amplitude. At 1200 K, the $\langle \delta r^2 \rangle_{\mathrm{Co}}$ increases linearly with the MMC step number. This behavior is due to a higher mobility of the Co atoms in the outer layers of the Co core that are strained by the Ag system. This result confirms that the outer Co layers, observed disordered, are liquid. The slope of $\langle \delta r^2 \rangle_{\mathrm{Co}}$ is higher at 1500 K indicating an increase of the average Co mobility. It is due to the higher number of Co atoms in the liquid phase. In order to characterize the influence of the cluster size and composition on the melting of Co cores, we define T_ϕ(Co) as the lowest temperature at which the Co subsystem is found totally molten. Figure 10 regroups the different value of T_ϕ(Co) as a function of the number of Co atoms in all studied clusters. T_ϕ(Co) increases with the number of Co atoms and keeps lower than the experimental melting temperature of bulk Co (1768 K). Remarkably, no influence of the thickness of the Ag shell can be seen in this graph, indicating that the melting temperature of the Co only depends on the number of Co atoms in the core. The weak influence of the Ag shell on the melting of Co is confirmed by the estimate of T_ϕ(Co) for elemental Co clusters, which dependence on size is the same as for mixed ones. In order to confirm the little influence of the Ag shell on the Co core melting, a better accurate estimate of T_ϕ(Co) is made for Co in an elemental Co_{200} cluster and in a $Ag_{1800}Co_{200}$ core-shell cluster. This latter mixed cluster contains 4 Ag layers inducing the largest strain in the Co core shown in Fig. 5. The evolution of $g(r)$ is reported in Fig. 11 for cobalt in both clusters at different temperatures around T_ϕ(Co). In the pair correlation function of both the elemental Co and the mixed clusters, the second, third and fourth neighbor peaks vanish at a temperature between 1000 K and 1100 K. The influence of the Ag layer is not sizable.

2. Lattice structure of the silver subsystem

a. Relaxation: Both the free surface and the Ag-Co interface induce a contraction of the silver lattice. Figure 12 shows the average first neighbor distance in the silver shell as a function of the Co concentration. Results are given for different cluster sizes. As expected, $d_{\mathrm{Ag\text{-}Ag}}$ is always lower in mixed clusters than in bulk Ag. For a given cluster size, increasing the Co concentration reduce strongly $d_{\mathrm{Ag\text{-}Ag}}$. The maximal contraction (about 4% of the bulk $d_{\mathrm{Ag\text{-}Ag}}$ value) is

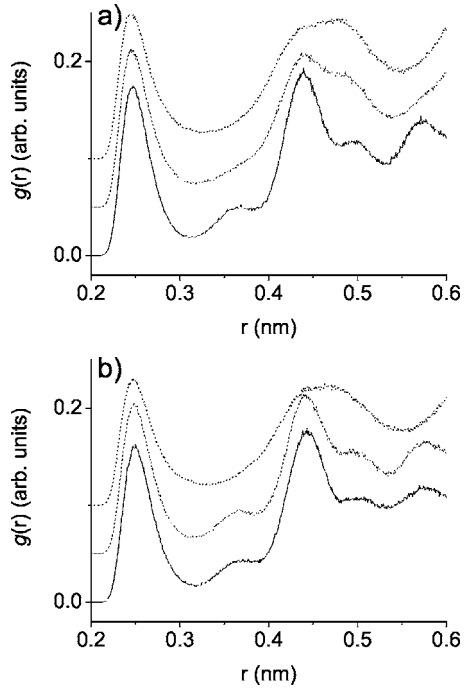

FIG. 11. Pair correlation functions associated with Co atoms at several temperatures around T_ϕ(Co). Solid line: 950 K; dashed line: 1000 K; dotted line: 1050 K. Results are displayed for (a) an elemental Co_{200} cluster and (b) the mixed $Ag_{1800}Co_{200}$ cluster.

observed for the smallest clusters with the largest Co concentration. Detail about the relation between the number of Co atoms and $d_{\mathrm{Ag\text{-}Ag}}$ comes out in Fig. 13, showing $d_{\mathrm{Ag\text{-}Ag}}$ as a function of the number of Co atoms in the core. The results are regrouped for clusters having the same number of Ag atomic layers but different sizes and thus different interfacial areas. The interfacial area, which is an increasing function of the number of Co atoms, turn out to have no significant influence on the relaxation of the Ag shell. On the other hand, the magnitude of the mean Ag contraction decreases with increasing number of Ag atomic layers, indicating that

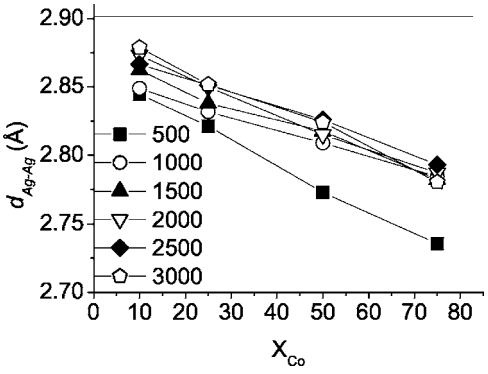

FIG. 12. The average Ag-Ag first neighbors distance, $d_{\mathrm{Ag\text{-}Ag}}$, as a function of the Co concentration in equilibrium mixed Ag-Co clusters at 300 K. Results for different cluster sizes are reported. The first neighbor distance in a bulk Ag single crystal at the same equilibrium temperature is given for comparison (horizontal line).

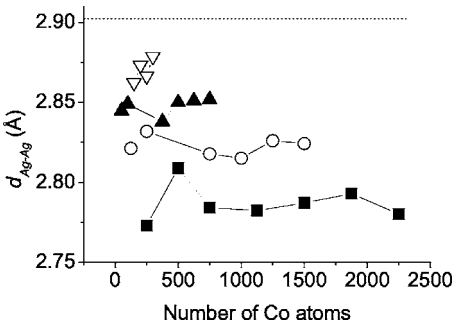

FIG. 13. $d_{\mathrm{Ag\text{-}Ag}}$ in mixed clusters as a function of the number of Co atoms. Results in clusters having 1, 2, 3, and 4 complete Ag atomic layers are represented, respectively, by squares, circles, triangles on the edge and on the tip. The dotted line represents the bulk Ag value.

the relaxation induced by the lattice mismatch at the Ag/Co interface is dominantly supported by the first Ag atomic layer. In clusters with more than four Ag atomic layers, the effect of the Co core is not sizable anymore and the relaxation is found close to the one observed in the elemental Ag clusters. In this case, the contribution of the free surface to contraction dominates.

b. Amorphization and melting: Amorphous nanoclusters are known at room temperature, often formed by alloying more than three elements.[52,53] Conditions for the amorphization of very small elemental metallic clusters are studied *ab initio*.[54] We here address the case of Ag shells covering Co cores. The problem is first examined for a given cluster size and size effects are considered next. In Fig. 14, the pair correlation functions of two clusters are compared, having the same size but different compositions, namely, $Ag_{2250}Co_{750}$ and $Ag_{1500}Co_{1500}$. The former has four Ag atomic layers and the latter two. As shown in the previous section, for a given size, increasing the Co concentration increases the relaxation in Ag. The consequences on the pair correlation function are seen on the second neighbor peak. This peak shows up in the four silver layers cluster at 300 K and 600 K and is absent in the $g(r)$ of the thinner silver layer, although the third and fourth neighbor peaks are present in both cases. At 900 K and higher, the second, third, and fourth peaks vanish, indicating a totally disordered state. As in the case of the Co core, a more detailed structural analysis of the crystalline state of the Ag shell inside the $Ag_{2250}Co_{750}$ cluster is made by estimating $g(r)$ inside concentric spherical layers having a thickness close to the first neighbor distance in Ag (2.82 Å). The results are shown in Fig. 15. At 300 K, $g(r)$ displays well-defined second, third, and fourth neighbor peaks in all Ag layers. At 600 K, all peaks are broader. The second neighbor peaks vanish in the outer layers while the inner layers still preserve a trace of the second, third, and fourth neighbors peaks. At 900 K, no Ag layers display any crystalline order. It thus turns out that the amorphous transformation of the Ag shell, characterized by the disappearance of the second neighbor peak, is due to the relaxations induced by the presence of the Co core but initiates at the free surface of the cluster and propagates inward

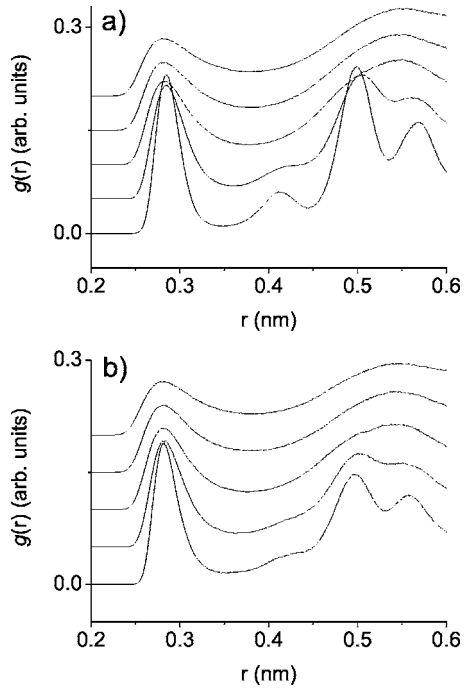

FIG. 14. $g(r)$ of the Ag subsystem in $Ag_{2250}Co_{750}$ and $Ag_{1500}Co_{1500}$ clusters at different temperatures: 300 K, 600 K, 900 K, 1200 K, and 1500 K. The lower curve corresponds to the lowest temperature.

as the temperature is increased. In order to distinguish between amorphous and liquid states, the mean square atomic displacements in the Ag shell are examined. $\langle \delta r^2 \rangle_{\mathrm{Ag}}$ is shown in Fig. 16 as a function of the MMC step number at different temperatures. At temperatures up to 600 K, $\langle \delta r^2 \rangle_{\mathrm{Ag}}$ is close to constant, indicating that the Ag shell is in the solid state. However, Figs. 14 and 15 show that the second neighbor peak vanishes at 600 K. The Ag shell is no more crystalline. This absence of both periodicity and diffusion is typical of the amorphous state. At 900 K, $\langle \delta r^2 \rangle_{\mathrm{Ag}}$ increases linearly with the step number. This, together with the lack of structure in $g(r)$ (Figs. 14 and 15), indicates the Ag liquid phase. As the pair correlation function is concerned, it thus appears necessary to distinguish one state where the second neighbor peaks vanishes, the amorphous state, from another where the longer distance peaks vanish too, the liquid state. Amorphization is caused by the increase with temperature of the lattice relaxation induced by the Co core and initiates at the cluster surface; melting is due to the additional contribution of thermal diffusion. The influence of size and composition on the amorphous and melting transitions in the Ag shell will now be explored. Similarly to the case of the Co cores, let us denote $T_{\phi}(\mathrm{Ag})$ the lowest temperature at which Ag is observed totally liquid. This temperature is 900 K in all the clusters considered, except for the smallest one (200 atoms) containing more than 10% Co, observed molten at 600 K. No influence of size or composition is observed. A possible influence of size or composition is thus only expected in the temperature range from 600 K to 900 K. Let us now define $T_{\alpha}(\mathrm{Ag})$ as the lowest temperature at which the second neigh-

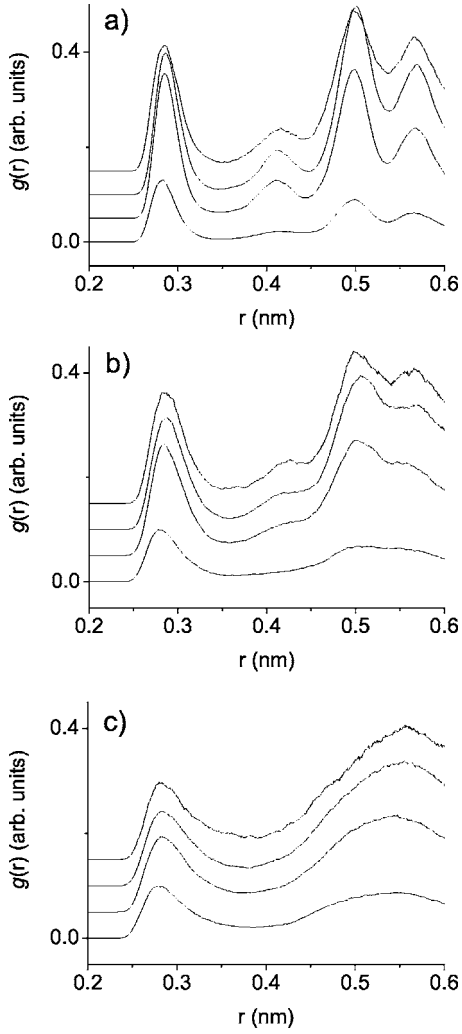

FIG. 15. $g(r)$ for Ag in different spherical layers with a thickness equal to 2.89 Å inside the $Ag_{2250}Co_{750}$ cluster. In each graph, the highest curve corresponds to the most inner atomic layer and the lowest to the upmost layer. The three different graphs a, b, and c are calculated, respectively, at 300 K, 600 K, and 900 K.

bor peak in $g(r)$ vanishes, but not the third and fourth peaks. $T_\alpha(\mathrm{Ag})$ is thus the lowest temperature at which the Ag shell can no more be considered as crystalline. Figure 17 gives $T_\alpha(\mathrm{Ag})$ as a function of number of Ag atomic layers. $T_\alpha(\mathrm{Ag})$

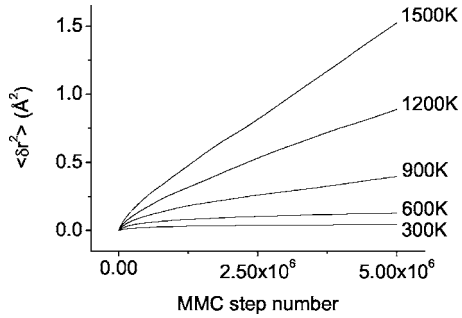

FIG. 16. Mean square displacement of Ag atoms, $\langle \delta r^2 \rangle_{\mathrm{Ag}}$, in a $Ag_{2250}Co_{750}$ equilibrium cluster at several different temperatures from 300 K to 1500 K.

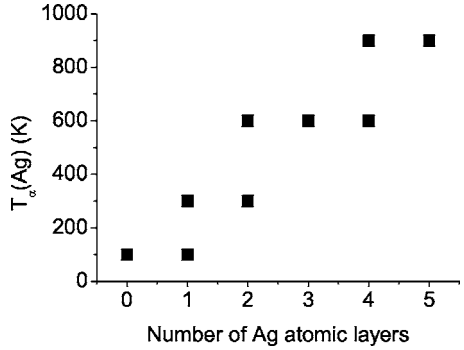

FIG. 17. $T_\alpha(\mathrm{Ag})$ as a function of the number of complete Ag atomic layers in the cluster.

is an increasing function of the number of atomic layers. In clusters containing more than 4 atomic layers, $T_\alpha(\mathrm{Ag})$ is equal to $T_\phi(\mathrm{Ag})$. For such clusters, no intermediate amorphization takes place and melting proceeds directly from the crystalline state. This is interpreted as resulting from the weakening of the average relaxation due to the Co/Ag interface as the thickness of the Ag shell is increased (see Fig. 13).

To summarize this section, the Ag shell is strongly affected by the relaxations induced by the presence of the Co core and the free surface. In the studied size range, the thickness of the Ag shell appears to be the main parameter governing the temperature dependence of the shell structure. As this thickness is increased, the influence of the Co core weakens and the Ag subsystem properties are closer to the properties of elemental Ag clusters. With increasing the temperature of the cluster, the Co core induces a crystal to amorphous transformation, which is followed by melting if the temperature is increased further. In all clusters considered, the silver shell is found molten at 900 K. This temperature is lower than the melting temperature of the Co cores, provided these cores contain more than 200 atoms (see Fig. 10) and leads to the prediction of possible core-shell structures with a solid core and a liquid shell.

IV. CONCLUSION

Several constrains govern the thermodynamic equilibrium state of free nanoparticles. In this report, size, composition and temperature are considered. The case study of Co-Ag particles is used that, thanks to synthesis methods far out of thermodynamic equilibrium conditions, may display, at the nanoscale, equilibrium compositions that cannot be met in bulk materials. This additional degree of freedom together with size effects opens the way to original equilibrium states, partially evidenced experimentally. An overall accurate picture is difficult to get for two reasons. The first is the number of state parameters (temperature, size, and composition) making complete phase diagrams complex. The second is the numerical nature of the approach used, requiring one long simulation for each set of parameter values. For instance, using six different temperatures, seven different sizes and compositions led us to run more than 294 simulations (rep-

resenting one year CPU time on a single processor). This way, the uncertainty on measured melting temperatures is 300 K. Reaching experimental accuracy in all thermodynamic conditions is presently out of the question. Nevertheless, an overall picture may be drawn and main lines are as follows. As configurations are concerned, the main feature is the core-shell structure. This one is encountered provided the following conditions are fulfilled. The total amount of Co atoms in the cluster must be larger than about 100 for the total Co binding energy to balance the energy stored in the deformation of the Ag system. Less than about 10 Co atoms form little groups just beneath the cluster surface at positions that may be influenced by the cluster morphology. The second condition is the need of a sufficient amount of silver in order to form at least one single monolayer around the Co core. When the amount of silver is lower, it wets the surface and a Frank-van der Merwe growth mode of Ag on the Co core surface is predicted possible. As cluster morphologies are concerned, the picture one gets from the present work is incomplete since the study of spherical clusters was privileged. In the case of small clusters however, a condition for faceting was evidenced, involving the cluster composition. The condition for faceting was not established for larger cluster sizes and probably depends on geometrical magic numbers as well as on composition. Nevertheless, extending the approach used with a small cluster to larger ones is straightforward. As cluster structures are concerned, one has to distinguish between the Co core and the Ag shell, having very different structural temperature dependencies. Owing to their small sizes, solid Co cores are fcc. When the temperature is increased, melting starts at the Ag-Co interface. The coexistence between a solid and a liquid phase within the Co core is predicted possible. The liquid Co surrounds the remaining solid core and the thickness of the liquid layer depends on temperature. The relation between its thickness and temperature could not be established and may involve a temperature range of a couple of hundred Kelvin. Two possible transitions are found at well distinct temperatures in the silver shell. The lowest transition temperature is crystal to amorphous and, when it is increased, amorphous to liquid. The temperature difference between these two transitions decreases with increasing shell thickness and vanishes when the thickness gets larger than four monolayers. In this case, the crystal-liquid transition is the only possible one. Although the crystal to amorphous transition finds its origin in the large lattice mismatch at the Ag-Co interface, it initiates at the Ag free surface and propagates inward as the temperature is increased. The melting temperature of the silver shell is lower than that of the Co core and the possibility of clusters with a solid core and a liquid shell is thus predicted. This sketch of thermodynamic properties of Co-Ag nanoparticles is based on MMC simulations using a semiempirical potential. The discussion of this potential is beyond the scope of this work and several elements, involving comparison with experiment, were already published. However, because of its semiempirical nature, new predictions can only be warranted by experimental confirmation. The core-shell nature of Ag-Co nanoparticles is an experimental fact. Their properties are however far from being explored, experimentally. Measurements on isolated particles are difficult because they have to be done on the fly. In addition, the possibilities of monitoring particle properties (like temperature) on the fly are limited. Therefore, the deposition of particles on surfaces may be necessary. This adds the bias of the interaction between the nanoparticles and the substrate. This interaction can be limited in the case of Co-Ag particles by using substrates, like carbon, assumed to have only weak interactions with the particles. However, the metal-carbon binding in such interactions is not well-known and its influence on the model uncertain. An alternative could be to use a substrate formed by one of the elements in the clusters and to include it into the model. This way, the same semiempirical potential would govern both the particle-surface interaction and the interactions between the particles. Hence, direct comparison between model and real experiments is foreseen realistic. A modelling program of Ag-Co clusters deposited on Ag(100) surfaces is already in progress.

[1] H. Haberland, *Clusters of Atoms and Molecules* (Springer-Verlag, Berlin, 1995).

[2] K. H. Meiwes-Broer, *Clusters on Surfaces* (Springer-Verlag, Berlin, 2000).

[3] L. W. Zhong, L. Yi, and S. Ze, *Handbook of Nanophase and Nanostructured Materials* (Kluwer Academic, New York, 2003).

[4] M. Schmidt and H. Haberland, C. R. Phys. **3**, 327 (2002).

[5] T. P. Martin, Phys. Rep. **273**, 199 (1996).

[6] S. Neukermans, E. Janssens, H. Tanaka, R. E. Silverans, and P. Lievens, Phys. Rev. Lett. **90**, 033401 (2003).

[7] B. Pauwels, G. Van Tendeloo, W. Bouwen, L. Theil Kuhn, P. Lievens, H. Lei, and M. Hou, Phys. Rev. B **62**, 10383 (2000).

[8] B. Pauwels, G. Van Tendeloo, E. Zhurkin, M. Hou, G. Verschoren, L. T. Kuhn, W. Bouwen, and P. Lievens, Phys. Rev. B **63**, 165406 (2001).

[9] C. L. Cleveland, W. D. Luedtke, and U. Landman, Phys. Rev. Lett. **81**, 2036 (1998).

[10] C. L. Cleveland, W. D. Luedtke, and U. Landman, Phys. Rev. B **60**, 5065 (1999).

[11] H. A. Duerr, S. S. Dhesi, E. Dudzik, D. Knabben, G. van der Laan, J. B. Goedkoop, and F. U. Hillebrecht, Phys. Rev. B **59**, R701 (1999).

[12] R. Rohlsberger, J. Bansmann, V. Senz, K. L. Jonas, A. Bettac, O. Leupold, R. Ruffer, E. Burkel, and K. H. Meiwes-Broer, Phys. Rev. Lett. **86**, 5597 (2001).

[13] P. Mélinon, V. Paillard, V. Dupuis, A. Perez, P. Jensen, A. Hoareau, J. P. Perez, J. Tuaillon, M. Broyer, J. L. Vialle, M. Pellarin, B. Baguenard, and J. Lerme, Int. J. Mod. Phys. B **139**, 339 (1995).

[14] W. Zhang, I. W. Boyd, N. S. Cohen, Q. T. Bui, Q. A. Pankhurst, M. Elliott, and W. Herrenden-Harkenrand, J. Appl. Phys. **81**, 5211 (1997).

[15] J. Guevara, A. M. Llois, and M. Weissmann, Phys. Rev. Lett. **81**, 5306 (1998).
[16] Yu. G. Pogorelov, G. N. Kakazei, and J. B. Sousa, Phys. Rev. B **60**, 12200 (1999).
[17] R. S. Iskhakov, S. V. Komogortsev, A. D. Balaev, and L. A. Chekanova, Tech. Phys. Lett. **28**, 725 (2002).
[18] E. Jcdryka, M. Ójcik, S. Nadolski, H. Pattyn, J. Verheyden, J. Dekoster, and A. Vantomme, J. Appl. Phys. **95**, 2770 (2004).
[19] J. Bansmann, S. H. Baker, C. Binns, J. A. Blackman, J-P. Bucher, J. Dorantes-Dàvila, V. Dupuis, L. Favre, D. Kechrakos, A. Kleibert, K-H. Meiwes-Broer, G. M. Pastor, A. Perez, O. Toutlemonde, K. N. Trohidou, J. Tuaillon, and Y. Xie, Surf. Sci. Rep. **56**, 189 (2005).
[20] A. S. Shirinyan and M. Wautelet, Nanotechnology **15**, 1720 (2004).
[21] R. L. Whetten, D. M. Cox, D. J. Travor, and A. Kaldor, Surf. Sci. **156**, 35 (1985).
[22] H. J. Fecht, Z. Metallkd. **94**, 1134 (2003).
[23] W. Bouwen, P. Thoen, F. Vanhoutte, S. Bouckaert, F. Despa, H. Weidele, R. E. Silverans, and P. Lievens, Rev. Sci. Instrum. **71**, 54 (2000).
[24] F. R. De Boer, R. Boom, W. C. M. Mattens, and A. R. Miedema, in *Cohesion in Metals*, edited by D. G. Petifor (Elsevier, Amsterdam, 1989).
[25] M. Gaudry, E. Cottancin, M. Pellarin, J. Lerm, L. Arnaud, J. R. Huntzinger, J. L. Vialle, M. Broyer, J. L. Rousset, M. Treilleux, and P. Mlinon, Phys. Rev. B **67**, 155409 (2003).
[26] L. Favre, S. Stanescu, V. Dupuis, E. Bernstein, T. Epicier, P. Mélinon, and A. Perez, Appl. Surf. Sci. **226**, 256 (2004).
[27] J. Tuaillon-Combes, O. Boisron, E. Bernstein, G. Guiraud, A. Gerbert, A. Milner, P. Mélinon, and A. Perez, Appl. Surf. Sci. **226**, 321 (2004).
[28] E. Janssens, S. Neukermans, P. Lievens, T. Van Hoof, and M. Hou (unpublished).
[29] E. Janssens, S. Neukermans, H. M. T. Nguyen, and P. Lievens (unpublished).
[30] F. Baletto, C. Mottet, and R. Ferrando, Phys. Rev. B **66**, 155420 (2002).
[31] F. Baletto, C. Mottet, and R. Ferrando, Phys. Rev. Lett. **90**, 135504 (2003).
[32] T. Van Hoof and M. Hou, Eur. Phys. J. D **29**, 33 (2004).
[33] M. P. Allen and D. J. Tildesley, *Computer Simulation in Liquids* (Oxford Science, Clarendon, 1987).
[34] D. Frenkel and B. Smit, *Understanding Molecular Simulation* (Academic, New York, 1996).
[35] M. S. Daw and M. I. Baskes, Phys. Rev. B **29**, 6443 (1984).
[36] J. H. Rose, J. R. Smith, F. Guinea, and J. Ferrante, Phys. Rev. B **29**, 2963 (1984).
[37] R. A. Johnson, Phys. Rev. B **41**, 9717 (1990).
[38] R. A. Johnson, Phys. Rev. B **39**, 12554 (1989).
[39] M. Hou, M. El Azzaoui, H. Pattyn, J. Verheyden, G. Koops, and G. Zhang, Phys. Rev. B **62**, 5117 (2000).
[40] W. H. Flores, S. R. Teixeira, J. Geshev, J. B. M. da Cunha, P. J. Shilling, A. Traverse, and M. C. Martins Alver, J. Magn. Magn. Mater. **188**, 17 (1998).
[41] R. Van Hardeveld and F. Hartog, Surf. Sci. **15**, 189 (1969).
[42] H. Haberland, in *Atomic Clusters and Nanoparticles*, Les Houches, edited by C. Guet, P. Hobza, and S. Spiegelman (Springer-Verlag, Berlin, 2001), Vol. 73.
[43] T. Castro, R. Reifenberger, E. Choi, and R. P. Andres, Phys. Rev. B **42**, 8548 (1990).
[44] M. Schmidt, R. Kusche, B. von Issendorff, and H. Haberland, Nature (London) **393**, 238 (1998).
[45] C. Rey, L. J. Gallego, J. Garcia-Rodeja, J. A. Alonso, and M. P. Iniguez, Phys. Rev. B **48**, 8253 (1993).
[46] J. Garcia-Rodeja, C. Rey, L. J. Gallego, and J. A. Alonso, Phys. Rev. B **49**, 8495 (1994).
[47] C. Rey, J. Garcia-Rodeja, L. J. Gallego, and M. J. Grimsun, Phys. Rev. E **57**, 4420 (1998).
[48] T. X. Li, Y. L. Ji, S. W. Yu, and G. H. Wang, Solid State Commun. **116**, 547 (2000).
[49] C. Mottet, J. Goniakowski, F. Baletto, R. Ferrando, and G. Treglia, Phase Transitions **77**, 101 (2004).
[50] A. Vichare and D. G. Kanhere, J. Phys.: Condens. Matter **10**, 3309 (1998).
[51] F. C. Chuang, C. Z. Wang, S. Ogut, J. R. Chelikowsky, and K. M. Ho, Phys. Rev. B **69**, 165408 (2004).
[52] A. Inoue, C. Fan, and A. Takeuchi, Mater. Sci. Forum **307**, 1 (1999).
[53] J. H. Perepezko, R. J. Herbert, and R. I. Wu, Mater. Sci. Forum **386–388**, 11 (2002).
[54] J. M. Soler, M. R. Beltrán, K. Michaelian, I. L. Garzón, P. Ordejón, D. Sánchez-Portal, and E. Artacho, Phys. Rev. B **61**, 5771 (2000).